nature chemistry

ARTICLES

PUBLISHED ONLINE: 20 JUNE 2016 | DOI: 10.1038/NCHEM.2549

Kinetic pathway for interfacial electron transfer from a semiconductor to a molecule

Ke Hu[1], Amber D. Blair[2], Eric J. Piechota[1], Phil A. Schauer[2], Renato N. Sampaio[1], Fraser G. L. Parlane[2], Gerald J. Meyer[1]* and Curtis P. Berlinguette[2]*

Molecular approaches to solar-energy conversion require a kinetic optimization of light-induced electron-transfer reactions. At molecular–semiconductor interfaces, this optimization has previously been accomplished through control of the distance between the semiconductor donor and the molecular acceptor and/or the free energy that accompanies electron transfer. Here we show that a kinetic pathway for electron transfer from a semiconductor to a molecular acceptor also exists and provides an alternative method for the control of interfacial kinetics. The pathway was identified by the rational design of molecules in which the distance and the driving force were held near parity and only the geometric torsion about a xylyl- or phenylthiophene bridge was varied. Electronic coupling through the phenyl bridge was a factor of ten greater than that through the xylyl bridge. Comparative studies revealed a significant bridge dependence for electron transfer that could not be rationalized by a change in distance or driving force. Instead, the data indicate an interfacial electron-transfer pathway that utilizes the aromatic bridge orbitals.

The ability to control charge-transfer events at illuminated semiconductor interfaces with a precision such as that known in molecular donor–bridge–acceptor compounds represents a goal of both practical importance and fundamental significance. In molecular compounds, superexchange can mediate electron transfer over long distances[1,2], whereas conjugated and/or redox-active bridges provide opportunities for electron hopping[3,4]. When the donor is a semiconductor and the acceptor is a molecule, the corresponding bridge chemistry remains unknown, even though control of this reaction is important for solar-cell optimization[5]. A distance dependence for this interfacial reaction has been demonstrated with molecular bridges[6–8] and in insulating thin films in core–shell nanoparticles[9,10], and is understood as an exponential decrease in the donor–acceptor electronic coupling, $H_{AB} = H^{o}_{AB}\exp(-\beta(R - R^{o})/2)$, where H^{o}_{AB} is the value of H_{AB} at the van der Waals separation R^{o} and β is a constant that scales the distance dependence[1]. However, the abstracted β values do not address whether the bridge simply fixes the distance over which the injected electron tunnels or whether specific pathways are operative. Reported herein is clear evidence of a specific electron-transfer 'pathway' for an interfacial electron transfer from a semiconductor to a molecule.

The question of whether specific electron-transfer pathways exist through the intervening matter that separates a donor from an acceptor has been considered for some time[11]. In some cases, it is now known that pathways do, indeed, exist[12–14]. For example, nature provides kinetic pathways for biological electron transfer that are now understood with a high level of sophistication[12,13,15,16]. Although a protein continuum β value of 1.4 $Å^{-1}$ provided reasonable estimates of long-range electron transfer in reaction centres[15,16], it is now understood that the details of the polypeptide structure as well as the presence of specific water clusters must be taken into account to rationalize fully the experimental data[12,13]. A 'tunnelling-pathway model' emerged for electron transfer in proteins and its educated use at molecular–semiconductor interfaces requires some experimental verification that such interfacial 'pathways' do exist. To date, models for electron transfer in molecular solar cells are based solely on thermodynamics and do not account for specific kinetic pathways that might exist. This is unfortunate as solar-cell efficiency is generally governed by kinetics and so the identification of pathways that both promote the desired electron transfers and inhibit unwanted reactions would be the most impactful.

How can specific electron-transfer pathways be identified at molecular–semiconductor interfaces? This is non-trivial and is not garnered easily from the previously mentioned 'distance-dependent' studies in which abstracted β values were subject to large uncertainties because of the limited range of distances possible in mesoporous TiO_2 thin films[6,7,9,10,17]. A further complication is that observed rate constants may not unambiguously report on the interfacial electron transfer of interest[18]. The acute sensitivity of this reaction to the number of TiO_2 electrons present in the nanocrystallite[17] and the very weak driving-force dependence reported by most[19–22], but not all[23], has led many to conclude that observed rate constants report only on the diffusional encounters of the TiO_2 electrons with the molecular acceptors[24–27]. Clifford *et al.* found that interfacial electron transfer was most easily understood when the physical location of the acceptor frontier molecular orbitals was taken into account[19], which has been exploited to optimize interfacial electron transfer with highly doped degenerate semiconductors[28]. Collectively, the prior literature is in line with the viewpoint that electron transfer from a semiconductor to a molecular acceptor is sensitive to distance, which naturally raises the question of whether specific interfacial pathways exist.

The experimental approach described here utilizes four bistridentate cyclometallated ruthenium(II) compounds linked to a pendent triphenylamine (TPA) group through either a xylyl- or a phenylthiophene bridge. When anchored to mesoporous nanocrystalline TiO_2 thin films, pulsed-light excitation is known to result in a rapid excited-state electron transfer to TiO_2 (refs 22,29) The desired reaction of the

[1]Department of Chemistry, The University of North Carolina at Chapel Hill, Murray Hall 2202B, Chapel Hill, North Carolina 27599-3290, USA. [2]Departments of Chemistry and Chemical & Biological Engineering, The University of British Columbia, 2036 Main Mall, Vancouver, British Columbia V6T1Z1, Canada. *e-mail: gjmeyer@email.unc.edu; cberling@chem.ubc.ca

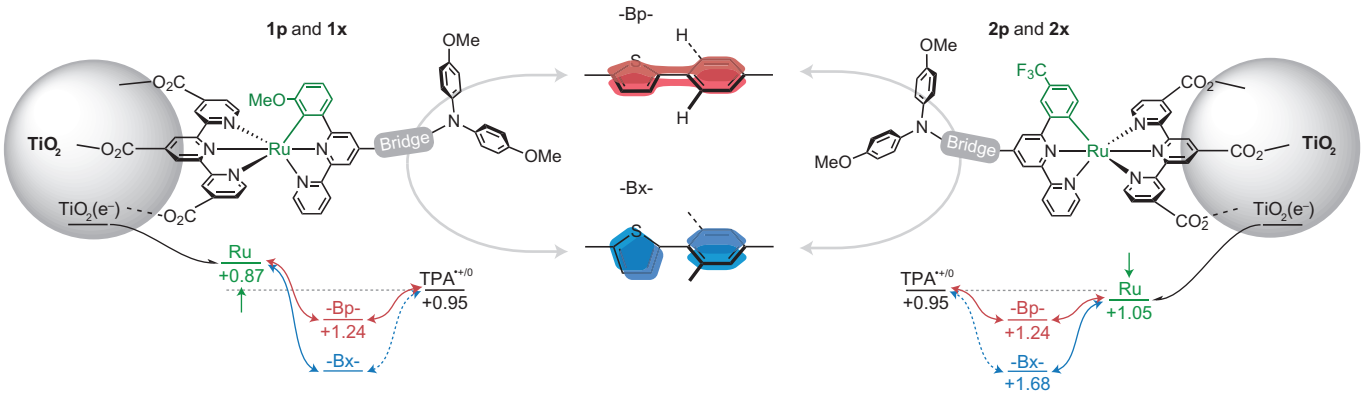

Figure 1 | The strategy utilized to demonstrate an electron-transfer pathway from TiO_2 to a molecule. Pulsed laser excitation initiates the excited-state injection that yields an electron in TiO_2 ($TiO_2(e^-)$) and an oxidized molecule. The subsequent reaction of the $TiO_2(e^-)$ with the oxidized molecule shown is then quantified on nanosecond and longer timescales. The exceptional aspect of these molecules is that they vary only in the geometric torsion about the aromatic bridge (grey), Bx = xylyl- or Bp = phenylthiophene. Hence, a bridge dependence for this reaction cannot be attributed to distance or driving force and must result from an interfacial electron-transfer pathway that utilizes the bridge orbitals.

$TiO_2(e^-)$ with Ru^{III} and $TPA^{\bullet+}$ can then be quantified on nanosecond and longer timescales (Fig. 1). Substituents on the cyclometallating ligand were used to tune the $Ru^{III/II}$ potential in two series of compounds that differed only in the bridging ligand, **1x** versus **1p** and **2x** versus **2p** where the **x** and **p** abbreviations indicate the xylyl and phenyl bridges. Within these series the distance and driving force is held essentially constant as the the nature of the bridge is varied. This approach was successful and the comparative study provides the first compelling evidence for an interfacial pathway and a clear demonstration that electron-transfer kinetics can be optimized through a judicious choice of the bridge. Such insights could not have been garnered had the distance and/or driving forces been changed.

Results

Spectroscopic and redox properties. The visible absorption spectra of the molecules anchored to the TiO_2 thin films were very similar to those measured for the carboxylate forms of the compounds in fluid solution. The materials absorb light through the visible region to beyond 800 nm in all cases. Owing to differences in the electronic coupling described further below, **1p** and **2p** have about twice the extinction coefficients of **1x** and **2x** (see Supplementary Fig. 1).

Spectroelectrochemistry was used to quantify the interfacial energetics in 0.5 M $LiClO_4/CH_3CN$ electrolyte (Fig. 2). Raising the Fermi level towards the vacuum level resulted in the reduction of TiO_2, with the characteristic appearance of the $TiO_2(e^-)$ absorption spectrum, as well as small shifts in the molecular absorption spectrum because of an electric-field effect[30]. Positive applied potentials resulted in absorption changes consistent with the sequential and reversible oxidation of the Ru centre and the TPA group; maintenance of isosbestic points enabled the determination of absorption spectra of the one- and two-electron oxidized states of these molecules. The integrated concentration change measured spectroscopically after a potential step of 15–25 mV is plotted as a capacitance in Fig. 2. The electron-donating $-OCH_3$ group on the aryl ring of the cyclometallating ligand for **1x** and **1p** lowered the $Ru^{III/II}$ reduction potential, whereas the electron-withdrawing $-CF_3$ group for **2x** and **2p** had the opposite effect. The $TPA^{\bullet+/0}$ reduction potentials were held constant by maintaining the same substituents for the entire series under evaluation. For **1x/TiO$_2$** the Ru metal centre was oxidized prior to the TPA group, whereas for **2x/TiO$_2$** the TPA donor was oxidized prior to the metal centre. The potential at which equal concentrations of the reduced and oxidized forms were present was taken as the $Ru^{III/II}$ and $TPA^{\bullet+/0}$ formal reduction potentials. The bridge unit had no measurable influence on the reduction potentials of **1x/TiO$_2$** relative to **1p/TiO$_2$**, and only a small 30 mV shift in the $Ru^{III/II}$ reduction potentials for **2x/TiO$_2$** relative to **2p/TiO$_2$** (Table 1).

Bridge-mediated electronic coupling. Analysis of the absorption spectra of the mixed-valent forms of these compounds generated by one-electron electrochemical oxidation was revealing. The appearance of an absorption band that was absent in the spectra of the ground and two-electron oxidized states was assigned to an intervalence charge-transfer (IVCT)-type transition (see Supplementary Figs 2 and 3). A weak absorption feature was observed for the mixed-valent form of **2x/TiO$_2$** at approximately the same energy as **2p/TiO$_2$**, but no IVCT band could be identified for **1x/TiO$_2$**. Operating within the approximations of the classic Marcus–Hush theory, the value of H_{AB} was calculated directly from the spectral band shape through the Mulliken–Hush expression (equation (1)):

$$H_{AB} = (4.2 \times 10^{-4} \varepsilon_{max} \Delta\nu_{1/2} E_{abs})^{1/2} / d \quad (1)$$

where ε_{max} ($M^{-1}\,cm^{-1}$) is the extinction coefficient of the IVCT band, $\Delta\nu_{1/2}$ (cm^{-1}) is the full-width at half-maximum (FWHM) of the Gaussian-shaped band, E_{abs} (cm^{-1}) is the energy of the transition maximum and d (Å) is the calculated 14 Å distance between the redox active Ru and the TPA centres[31,32]. This analysis revealed an H_{AB} value of about $1{,}800 \pm 200\ cm^{-1}$ for **1p/TiO$_2$**, $1{,}000 \pm 300\ cm^{-1}$ for **2p/TiO$_2$** and $<100\ cm^{-1}$ for **2x/TiO$_2$**. The inability to resolve the IVCT band for **1x/TiO$_2$** also implies a weak electronic coupling with $H_{AB} < 100\ cm^{-1}$. Although details of the IVCT energies and band shapes deserve further study, this analysis supports the hypothesis that the methyl substituents in the xylyl bridge disrupt the arylthiophene-bridge conjugation and thereby decrease H_{AB}.

Time-resolved absorption spectroscopy. Figure 3a displays absorption-difference spectra measured at the indicated delay times after pulsed-laser excitation of **2x/TiO$_2$**. The corresponding data for **1x/TiO$_2$** is given in Supplementary Fig. 4. The absorption band centred at 740 nm was characteristic of $TPA^{\bullet+}$ and the metal-to-ligand charge-transfer (MLCT) bleach was diagnostic of the oxidized Ru chromophore. Contributions from the excited states were negligible and spectral simulations based on the spectroelectrochemical data were found to model the transient data accurately, which allowed the relative concentrations of Ru^{III} and $TPA^{\bullet+}$ to be quantified at all times after laser excitation. The prompt appearance of the oxidized molecules indicated a rapid

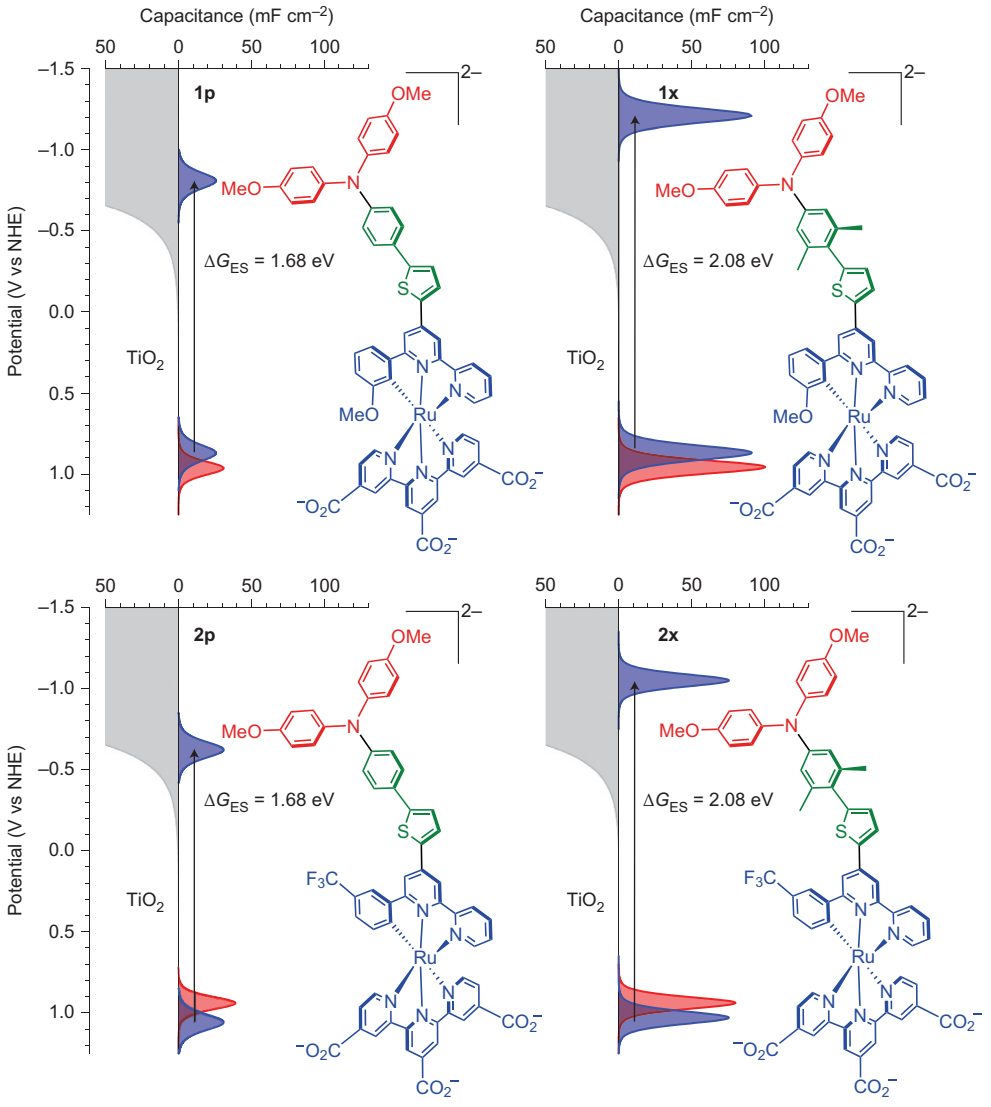

Figure 2 | The interfacial density of states for 1p/TiO_2, 1x/TiO_2, 2p/TiO_2 and 2x/TiO_2. The distributions at positive potentials were abstracted from spectroelectrochemical data measured in 0.5 M $LiClO_4$/CH_3CN. The distributions shaded in blue correspond to $Ru^{III/II}$ redox equilibria and those shaded in red correspond to $TPA^{\bullet+/0}$. The free energy stored in the excited states, ΔG_{ES}, was subtracted from the $Ru^{III/II}$ distributions to estimate the excited-state reduction potentials that were found to overlap with the TiO_2 acceptor states that are shaded in grey.

excited-state electron injection, $k_{inj} > 10^8\ s^{-1}$ in all cases. Comparative studies with *cis*-Ru(dcb)$_2$(NCS)$_2$-sensitized TiO_2 (dcb, 2,2′-bipyridine-4,4′-dicarboxylic acid) revealed that the injection yields were near unity. For the xylyl-bridged sensitizers, about 15% of the $TPA^{\bullet+}$ signal increase was time resolved, consistent with nanosecond $Ru^{III} \rightarrow TPA$ hole transfer, $k_{ht} = 2 \times 10^8\ s^{-1}$. The appearance of $TPA^{\bullet+}$ for the phenyl-bridged molecules required picosecond time resolution and was about an order of magnitude faster, $k_{ht} = 4 \times 10^9\ s^{-1}$ (Supplementary Fig. 5).

Electron-transfer kinetics. Visual inspection of the data in Fig. 3a reveals that the bleach associated with Ru^{III} returns to pre-excitation levels on a faster timescale than does the long-wavelength absorption caused by $TPA^{\bullet+}$. Similar observations were made after pulsed-light excitation of **1x/TiO_2**. In contrast, recombination to Ru^{III} and $TPA^{\bullet+}$ occurred simultaneously for the phenyl-bridged sensitizers such that the normalized absorption-difference spectra were time independent.

The kinetics for interfacial electron transfer to yield ground-state products are non-exponential and satisfactorily fit to a sum of two Kohlrausch–Williams–Watts (KWW) functions (equation (2))[33]:

$$\Delta A(\lambda,t) = A_{Ru^{III}}(\lambda)e^{-(k_{Ru^{III}}t)^{\beta}} + A_{TPA^{\bullet+}}(\lambda)e^{-(k_{TPA^{\bullet+}}t)^{\beta}} \quad (2)$$

$$\bar{k} = \left[\frac{1}{k\beta} \times \Gamma\left(\frac{1}{\beta}\right)\right]^{-1} \quad (3)$$

In these expressions, β is related to the breadth of an underlying Lévy distribution of rate constants. The average rate constant, $\bar{k}$, was calculated as the first moment (equation (3))[34]. The wavelength-dependent amplitudes $A_{Ru^{III}}$ and $A_{TPA^{\bullet+}}$ were linked to a specific rate constant and plotted against the observation wavelength to yield decay-associated spectra (DAS) for the two components[35]. Typical DAS are given in Fig. 3b with $\bar{k}_{Ru^{III}} = 6.2 \pm 0.6 \times 10^5\ s^{-1}$ and $\bar{k}_{TPA^{\bullet+}} = 1.7 \pm 0.2 \times 10^4\ s^{-1}$. The DAS spectra thus provided clear evidence that the two kinetic processes were the reduction of the Ru^{III} or $TPA^{\bullet+}$ groups. Charge recombination to give a Ru model compound that did not contain a pendant TPA donor occurred with an average rate constant of $\bar{k}_{Ru^{III}} = 1.9 \pm 0.2 \times 10^4\ s^{-1}$.

Table 1 | $E_{1/2}$, k and H_{AB} for compounds anchored to TiO_2.

Compounds	$E_{1/2}$* ($Ru^{III/II}$)	$E_{1/2}$* ($TPA^{\bullet+/0}$)	$\bar{k}_{Ru^{III}}$ (10^5 s^{-1})	$\bar{k}_{TPA^{\bullet+}}$ (10^5 s^{-1})	H_{AB}† (cm^{-1})
1x/TiO_2	870	960	5.4‖	0.51‖	<100
1p/TiO_2	870	960	0.19¶	0.19¶	1,800
2x/TiO_2	1,030	940	6.2‖	0.17‖	<100
2p/TiO_2	1,060	940	0.19¶	0.19¶	1,000

*Potentials are in mV vs NHE. †The values for 1p/TiO_2 and 2p/TiO_2 were abstracted from IVCT analysis of the mixed-valent form of the compound, and the values for the xylyl-bridged sensitizers are set as lower limits (see the Supplementary Information). ‖Values abstracted from fits to equation (2) with $\beta = 0.19$. ¶Calculated with $\beta = 0.26$, which corresponds to recombination to the equilibrium system (see text).

Single-wavelength kinetics monitored at the peak maximum of 750 nm for $TPA^{\bullet+}$ and 510 nm (or 540 nm) for Ru^{III} with overlaid fits are given in Fig. 3c,d. The kinetic data measured between 510 and 540 nm represent a bleach that is inverted in Fig. 3 to aid comparisons. These kinetic data are distinctly different to those of **1p/TiO_2** and **2p/TiO_2**, for which the abstracted rate constants were the same within experimental error (Fig. 3c,d insets)[29].

Discussion

The spectroscopic and electrochemical data clearly indicate that the approach described above for the identification of an interfacial electron-transfer pathway was successful. To a very good approximation the thermodynamics and distance for interfacial electron transfer were held at parity, with only the nature of the intervening bridge being altered. Significantly, the $E^o(TPA^{\bullet+/0})$ reduction potentials were the same for all the compounds studied. Density functional theory (DFT) indicated that the methyl substituents in the xylyl bridge destabilized the planar configuration of the arylthiophene moiety by about 40 kJ mol^{-1} relative to the phenyl bridge. The extinction coefficients of the xylyl-bridged compounds were about half those with phenyl bridges, a behaviour that is also consistent with decreased conjugation[36,37]. Marcus–Hush analysis of the absorption spectra of the one-electron oxidized forms of these molecules revealed an approximate tenfold decrease in electronic coupling (H_{AB}) through the xylyl bridge. The important role that electronic coupling plays in interfacial electron transfer was revealed by kinetic experiments in which a laser pulse was used to inject electrons into TiO_2 and the subsequent electron transfer to the singly oxidized molecules was quantified.

For the phenyl-bridged molecules, electron transfers to the remote $TPA^{\bullet+}$ and the more proximate Ru^{III} centre were identical. The kinetics were non-exponential, yet overlaid raw transient data as well as average rate constants revealed that the electron transfer to both acceptors was the same, $\bar{k}_{Ru^{III}}/\bar{k}_{TPA^{\bullet+}} = 1$. Strong electronic coupling, $H_{AB} > 1{,}000$ cm^{-1}, provides highly delocalized molecular orbitals that promote a rapid adiabatic electron transfer. At such a strongly coupled interface there is no kinetic advantage for a Ru^{III} → TPA hole transfer; however, the larger

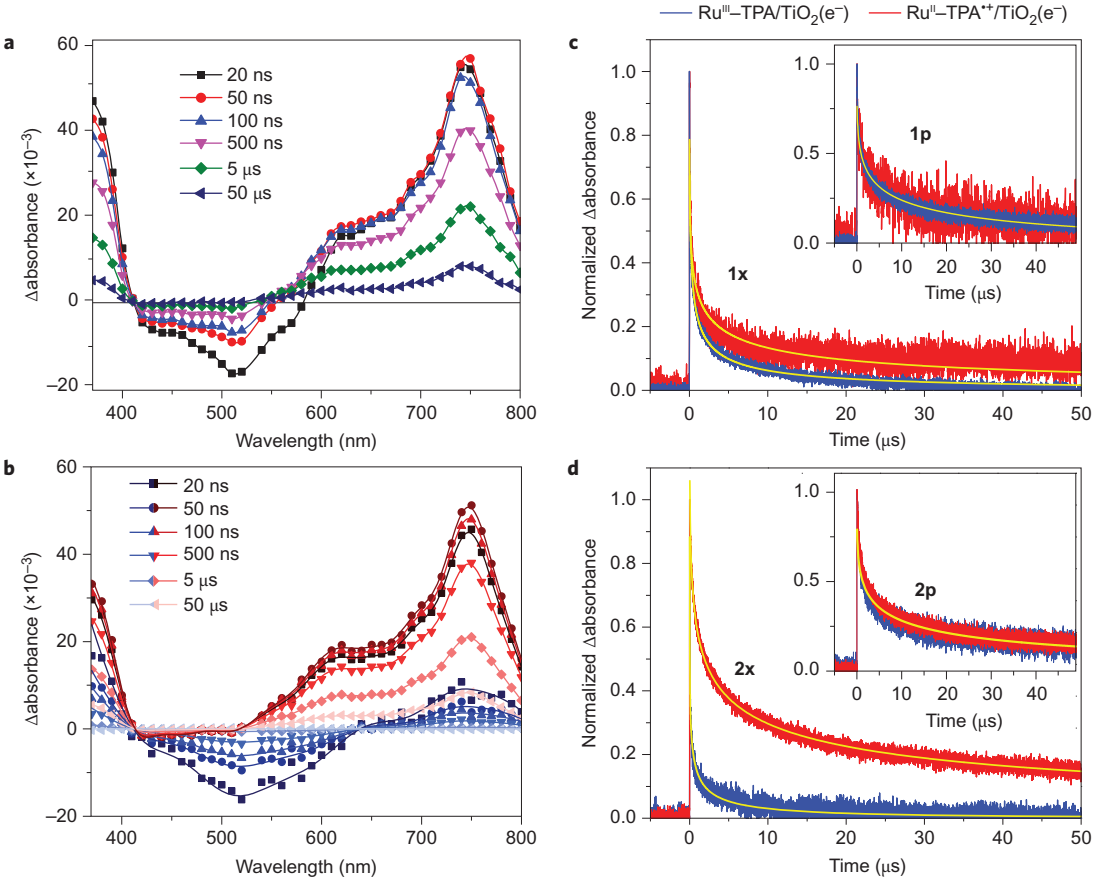

Figure 3 | Spectroscopic and kinetic evidence of a pathway for interfacial electron transfer from TiO_2 to the remote $TPA^{\bullet+}$. a, The transient-absorption-difference spectra measured at the indicated delay times after pulsed 532 nm excitation (0.4 mJ cm^{-2}) of **2x/TiO_2** in 0.5 M $LiClO_4/CH_3CN$. **b**, The DAS abstracted from the data in **a** reveal how the Ru^{III} (blue) and $TPA^{\bullet+}$ (red) concentrations change with time. **c,d**, Single-wavelength kinetic data monitored at wavelengths that predominately report on electron transfer from TiO_2 to Ru^{III} (blue) or $TPA^{\bullet+}$ (red) with overlaid fits to the KWW function. The comparative kinetic analysis shows that the reductions of $TPA^{\bullet+}$ and Ru^{III} were the same for the phenyl bridge, $\bar{k}_{Ru^{III}}/\bar{k}_{TPA^{\bullet+}} = 1$, and were significantly influenced by the xylyl bridge, $\bar{k}_{Ru^{III}}/\bar{k}_{TPA^{\bullet+}} > 10$.

surface dipole formed when the TPA is oxidized is known to enhance open-circuit photovoltages[22].

In contrast with the phenyl-bridged molecules, electron transfer to the remote $TPA^{\bullet+}$ was slow relative to electron transfer to Ru^{III} for the xylyl-bridged compounds, $\bar{k}_{Ru^{III}}/\bar{k}_{TPA^{\bullet+}} > 10$. Indeed, after pulsed-laser excitation of **2x**/**TiO$_2$**, electron transfer to the remote $TPA^{\bullet+}$ was the only kinetic process observed at long observation times. Theoretical calculations indicate that the xylylthiophene-bridge molecular orbitals were further removed from the $Ru^{III/II}$ and $TPA^{\bullet+/0}$ reduction potentials than were those of the phenylthiophene bridge, which resulted in decreased mixing and more-localized molecular orbitals. A Marcus–Hush analysis of the mixed valent forms directly indicates a weak electronic coupling through the xylyl bridge, $H_{AB} < 100\ cm^{-1}$, which probably underlies the temporal data.

The kinetic data indicate that observed rate constants do, indeed, report on interfacial electron transfer and are not rate limited by diffusional encounters of the injected electron and the oxidized sensitizer. A preliminary temperature-dependent study revealed a significant barrier, the details of which will be reported elsewhere. Given the homologous nature of these molecules and the parity of the $TPA^{\bullet+/0}$ reduction potentials, it is clear that the pathway for electrons includes transfer through the bridge orbitals. The use of methyl substituents that sterically prevent planarization and lower electronic couplings in molecular donor–bridge–acceptor compounds has been exploited previously in molecular energy transfer[38], thermal electron transfer[39] and light-driven electron transfer[40–43]. This is the first example at an interface and is important for controlling electron transfer at illuminated semiconductor interfaces that does not necessitate the loss of free energy or rely on distance.

Prior reports and DFT analysis indicate that the direct oxidation or reduction of the bridge through a 'hopping mechanism' can be ruled out under these experimental conditions[44]. The lowest-energy bridge-dominated unfilled molecular orbitals are >3 eV, whereas the filled molecular orbitals are within 1 eV of the $Ru^{III/II}$ and $TPA^{\bullet+/0}$ reduction potentials. This suggests that electron transfer occurs by a 'hole'-transfer superexchange mechanism with the filled bridge orbitals. This mechanism is well established in purely molecular compounds and has recently been shown to support long-range electronic communication over distances of >27 Å through an oligophenylene bridge that provides an electronic coupling intermediate to that reported here for the xylyl- and phenylthiophene bridges[44]. Although there would be no kinetic advantage to hole superexchange through an oligophenylene bridge immobilized on semiconductor surfaces, the data reported here indicate that this bridge would also provide a pathway for electron transfer over large distances.

Conclusion

The spectroscopic and redox behaviours of a homologous series of four rigid molecules anchored to semiconducting mesoporous TiO_2 thin films were quantified. The electronic coupling was tuned by the introduction of methyl groups that inhibited the planarization of a thiophene unit with an aromatic ring of a triarylamine donor. DFT indicated that the coplanar geometry was destabilized by 40 kJ mol^{-1}; Marcus–Hush analysis of the IVCT absorption bands revealed that H_{AB} decreased by about a factor of ten. The orientation of the arylthiophene bridge was found to influence significantly the electron transfer from TiO_2 to a distal acceptor and thereby provide the first compelling evidence of a pathway for this important interfacial reaction. These data reveal that through-bond pathways need to be considered in the development of fundamental mechanistic models for interfacial electron transfer at molecular–semiconductor interfaces. Furthermore, the molecular arrangement of the bridge atoms can have a dramatic influence on interfacial electron transfer that can be exploited to optimize the efficiency of solar-energy conversion. Although enhancing conjugation in donor–bridge–acceptor sensitizers has been a uniform goal of practitioners seeking state-of-the-art devices over the past half-decade, this work shows for the first time the possible benefit of disrupting the said conjugation.

Methods

Synthetic procedures. All the synthetic procedures are detailed in Supplementary Methods 1.

Sensitized thin films. Mesoporous nanocrystalline TiO_2 thin films were prepared as described previously[45]. The as-prepared TiO_2 thin films were immersed in ~1×10^{-4} M solution of the compounds over 12 hours for saturation surface coverage for the spectroelectrochemistry. The absorbance of the film was controlled at ~0.4 at 532 nm for transient-absorption measurements in the transmission mode. All the samples were purged with argon gas for at least 30 minutes prior to experimentation.

Spectroelectrochemistry. Steady-state ultraviolet–visible (UV-vis) absorption measurements were carried out on a Varian Cary 50 spectrophotometer at room temperature. Potential steps were applied by a BAS model CV-50W potentiostat. Sensitized TiO_2 thin films on fluorine-doped tin oxide glass (15 Ω per square) were used as the working electrodes, along with a AgCl/Ag pseudoreference electrode and a platinum-disk counter electrode; the electrodes were positioned in a 1 cm quartz cuvette and used as the standard three-electrode cell. The pseudoreference electrode was calibrated against a ferrocenium/ferrocene (Fc^+/Fc) standard before and after the experiments and was converted into a normal hydrogen electrode (NHE) with the Fc^+/Fc half-wave potential of +630 mV versus (vs) NHE[46].

Transient-absorption spectroscopy. Nanosecond transient-absorption measurements were obtained on an apparatus similar to that described previously[45]. Briefly, samples were excited by a frequency-doubled Q-switched pulsed neodymium-doped yttrium–aluminium–garnet laser (Quantel USA (BigSky) Brilliant B; 532 nm, 5–6 ns FWHM, 1 Hz, ~1 cm in diameter) at ~45° to the thin-film substrate surface. A 150 W Xe arc lamp (Applied Photophysics) served as the probe beam orthogonal to the excitation direction. Detection was achieved by a R928 photomultiplier tube (Hamamatsu) optically coupled to a monochromator (Spex 1702/04). Transient data were acquired using a computer-interfaced digital oscilloscope (LeCroy 9450, Dual 350 MHz). Transient signals were typically averaged with 30–50 laser pulses. Kinetic-data fitting was performed in Origin 9 using the Levenberg–Marquardt iteration method for least-squares error minimization, and spectral modelling was performed using a code written in Mathematica 10. Excited-state injection yields for all the compounds were determined by comparative actinometry using *cis*-$Ru(dcb)_2(NCS)_2$ as the reference with an injection yield equal to one (Supplementary Table 1[47]).

DFT calculations. Ground-state geometries of the xylyl- and phenylthiophene bridges were optimized and the orbital energies were calculated using B3LYP and the 6-31G(d) basis set. The calculation was carried using the Gaussian 09 Package[48].

H_{AB} calculation. Using equation (1), H_{AB} was calculated individually for both **1p** and **2p**.

2p. The growth and recession of a charge-transfer band was evident in the steady-state UV-vis spectroelectrochemical data, but was analysed explicitly by subtracting the ground-state spectrum at an applied potential that could not oxidize TPA or the Ru^{II} centre (see above (Fig. 1)). After the various spectra at higher applied potentials were subtracted from the ground state, we observed a bleach of the MLCT absorbance at 530 nm and a growth of $TPA^{\bullet+}$ absorbance that occurred at around 730 nm. There was a significant growth and decay of an absorbance peak to the high-energy side of the formal $TPA^{\bullet+}$ absorbance attributed to an IVCT band. This band, centred at 15,500 cm^{-1} (645 nm), reached a maximum at 995 mV vs NHE. Five unique Gaussian fits of the band yielded values for E_{abs} (*vide supra*) and $\Delta\nu_{1/2}$. ε_{max} was estimated from the extinction coefficient of a structurally similar compound at 19,230 cm^{-1} (520 nm) and 23,200 cm^{-1} (431 nm) with extinction coefficients of 41.5×10^3 and 39.1×10^3 M^{-1} cm^{-1}, respectively[49]. Under the assumption that the number of **2p** molecules in the intervalence state is equal to the number in the ground state (that is, a complete one e^- oxidation to the mixed valence state), a ratio of absorbance values and extinction coefficients was employed, and ten values of H_{AB} were calculated. The average of these values is reported in Table 1.

1p. A similar analysis was performed for **1p**. The growth occurred at energies similar to the bleach of the ground state of **1p**, which complicated the analysis when the ground state was used as a reference spectrum. To circumvent this, the fully oxidized

spectrum was treated as the ground state of the system. A depletion of $TPA^{\bullet+}$ absorbance at 740 nm and a growth of the Ru^{II}-centred absorbance at 530 nm were observed. Similar to **2p**, the growth and recession of a band was attributed to an IVCT transition. The band maximum was observed at 905 mV vs NHE, and was centred at 20,620 cm^{-1} (485 nm). The extinction coefficients used for the structural analogue of **1p** were observed at 18,800 cm^{-1} (532 nm) and 22,780 cm^{-1} (439 nm) with reported values of 32.8×10^3 and 44.9×10^3 M^{-1} cm^{-1}, respectively[49]. The approach used to calculate the IVCT extinction for **1p** was the same as that for **2p**. The average value is given in Table 1.

Received 25 November 2015; accepted 10 May 2016; published online 20 June 2016

References

1. Closs, G. L. & Miller, J. R. Intramolecular long-distance electron transfer in organic molecules. *Science* **240,** 440–447 (1988).
2. Davis, W. B., Svec, W. A., Ratner, M. A. & Wasielewski, M. R. Molecular-wire behaviour in *p*-phenylenevinylene oligomers. *Nature* **396,** 60–63 (1998).
3. Lambert, C., Noll, G. & Schelter, J. Bridge-mediated hopping or superexchange electron-transfer processes in bis(triarylamine) systems. *Nature Mater.* **1,** 69–73 (2002).
4. Vura-Weis, J. *et al.* Crossover from single-step tunneling to multistep hopping for molecular triplet energy transfer. *Science* **328,** 1547–1550 (2010).
5. Ardo, S. & Meyer, G. J. Photodriven heterogeneous charge transfer with transition-metal compounds anchored to TiO_2 semiconductor surfaces. *Chem. Soc. Rev.* **38,** 115–164 (2009).
6. Abrahamsson, M. *et al.* Decreased interfacial charge recombination rate constants with N3-type sensitizers. *J. Phys. Chem. Lett.* **1,** 1725–1728 (2010).
7. Asbury, J. B., Hao, E. C., Wang, Y. Q. & Lian, T. Q. Bridge length-dependent ultrafast electron transfer from Re polypyridyl complexes to nanocrystalline TiO_2 thin films studied by femtosecond infrared spectroscopy. *J. Phys. Chem. B* **104,** 11957–11964 (2000).
8. Haque, S. A. *et al.* Supermolecular control of charge transfer in dye-sensitized nanocrystalline TiO_2 films: towards a quantitative structure–function relationship. *Angew. Chem. Int. Ed.* **44,** 5740–5744 (2005).
9. Cameron, P. J. & Peter, L. M. Characterization of titanium dioxide blocking layers in dye-sensitized nanocrystalline solar cells. *J. Phys. Chem. B* **107,** 14394–14400 (2003).
10. Palomares, E., Clifford, J. N., Haque, S. A., Lutz, T. & Durrant, J. R. Control of charge recombination dynamics in dye sensitized solar cells by the use of conformally deposited metal oxide blocking layers. *J. Am. Chem. Soc.* **125,** 475–482 (2003).
11. Taube, H. & Myers, H. Evidence for a bridged activated complex for electron transfer reactions. *J. Am. Chem. Soc.* **76,** 2103–2111 (1954).
12. Beratan, D. N., Betts, J. N. & Onuchic, J. N. Protein electron transfer rates set by the bridging secondary and tertiary structure. *Science* **252,** 1285–1288 (1991).
13. Beratan, D. N., Onuchic, J. N., Winkler, J. R. & Gray, H. B. Electron-tunneling pathways in proteins. *Science* **258,** 1740–1741 (1992).
14. Wenger, O. S. Photoinduced electron and energy transfer in phenylene oligomers. *Chem. Soc. Rev.* **40,** 3538–3550 (2011).
15. Hopfield, J. J. Electron transfer between biological molecules by thermally activated tunneling. *Proc. Natl Acad. Sci. USA* **71,** 3640–3644 (1974).
16. Moser, C., Page, C., Farid, R. & Dutton, P. L. Biological electron transfer. *J. Bioenerg. Biomembr.* **27,** 263–274 (1995).
17. Haque, S. A., Tachibana, Y., Klug, D. R. & Durrant, J. R. Charge recombination kinetics in dye-sensitized nanocrystalline titanium dioxide films under externally applied bias. *J. Phys. Chem. B* **102,** 1745–1749 (1998).
18. Brigham, E. C. & Meyer, G. J. Ostwald isolation to determine the reaction order for $TiO_2(e^-)|S^+ \rightarrow TiO_2|S$ charge recombination at sensitized TiO_2 interfaces. *J. Phys. Chem. C* **118,** 7886–7893 (2014).
19. Clifford, J. N. *et al.* Molecular control of recombination dynamics in dye-sensitized nanocrystalline TiO_2 films: free energy vs distance dependence. *J. Am. Chem. Soc.* **126,** 5225–5233 (2004).
20. Hasselmann, G. M. & Meyer, G. J. Diffusion-limited interfacial electron transfer with large apparent driving forces. *J. Phys. Chem. B* **103,** 7671–7675 (1999).
21. Maggio, E. & Troisi, A. Theory of the charge recombination reaction at the semiconductor–adsorbate interface in the presence of defects. *J. Phys. Chem. C* **117,** 24196–24205 (2013).
22. Hu, K. *et al.* Intramolecular and lateral intermolecular hole transfer at the sensitized TiO_2 interface. *J. Am. Chem. Soc.* **136,** 1034–1046 (2014).
23. Kuciauskas, D., Freund, M. S., Gray, H. B., Winkler, J. R. & Lewis, N. S. Electron transfer dynamics in nanocrystalline titanium dioxide solar cells sensitized with ruthenium or osmium polypyridyl complexes. *J. Phys. Chem. B* **105,** 392–403 (2001).
24. Ashford, D. L. *et al.* Photoinduced electron transfer in a chromophore–catalyst assembly anchored to TiO_2. *J. Am. Chem. Soc.* **134,** 19189–19198 (2012).
25. Barzykin, A. V. & Tachiya, M. Mechanism of molecular control of recombination dynamics in dye-sensitized nanocrystalline semiconductor films. *J. Phys. Chem. B* **108,** 8385–8389 (2004).
26. Hanson, K. *et al.* Structure–property relationships in phosphonate-derivatized, Ru^{II} polypyridyl dyes on metal oxide surfaces in an aqueous environment. *J. Phys. Chem. C* **116,** 14837–14847 (2012).
27. Nelson, J. Continuous-time random-walk model of electron transport in nanocrystalline TiO_2 electrodes. *Phys. Rev. B* **59,** 15374–15380 (1999).
28. Huang, Z. J. *et al.* Dye-controlled interfacial electron transfer for high-current indium tin oxide photocathodes. *Angew. Chem. Int. Ed.* **54,** 6857–6861 (2015).
29. Hu, K., Robson, K. C. D., Johansson, P. G., Berlinguette, C. P. & Meyer, G. J. Intramolecular hole transfer at sensitized TiO_2 interfaces. *J. Am. Chem. Soc.* **134,** 8352–8355 (2012).
30. Ardo, S., Sun, Y., Staniszewski, A., Castellano, F. N. & Meyer, G. J. Stark effects after excited-state interfacial electron transfer at sensitized TiO_2 nanocrystallites. *J. Am. Chem. Soc.* **132,** 6696–6709 (2010).
31. Brunschwig, B. S., Creutz, C. & Sutin, N. Optical transitions of symmetrical mixed-valence systems in the Class II–III transition regime. *Chem. Soc. Rev.* **31,** 168–184 (2002).
32. Chen, P. Y. & Meyer, T. J. Medium effects on charge transfer in metal complexes. *Chem. Rev.* **98,** 1439–1477 (1998).
33. Williams, G. & Watts, D. C. Non-symmetrical dielectric relaxation behaviour arising from a simple empirical decay function. *Trans. Faraday Soc.* **66,** 80–85 (1970).
34. Lindsey, C. P. & Patterson, G. D. Detailed comparison of the Williams–Watts and Cole–Davidson functions. *J. Chem. Phys.* **73,** 3348–3357 (1980).
35. Knutson, J. R., Walbridge, D. G. & Brand, L. Decay-associated fluorescence spectra and the heterogeneous emission of alcohol-dehydrogenase. *Biochemistry* **21,** 4671–4679 (1982).
36. Robson, K. C. D., Koivisto, B. D., Gordon, T. J., Baumgartner, T. & Berlinguette, C. P. Triphenylamine-modified ruthenium(II) terpyridine complexes: enhancement of light absorption by conjugated bridging motifs. *Inorg. Chem.* **49,** 5335–5337 (2010).
37. Chen, C.-Y. *et al.* Multifunctionalized ruthenium-based supersensitizers for highly efficient dye-sensitized solar cells. *Angew. Chem. Int. Ed.* **47,** 7342–7345 (2008).
38. Song, H. E. *et al.* Linker dependence of energy and hole transfer in neutral and oxidized multiporphyrin arrays. *J. Phys. Chem. B* **113,** 16483–16493 (2009).
39. Chen, P. Y., Curry, M. & Meyer, T. J. Effects of conformational change in the acceptor on intramolecular electron transfer. *Inorg. Chem.* **28,** 2271–2280 (1989).
40. Hanss, D., Walther, M. E. & Wenger, O. S. Importance of covalence, conformational effects and tunneling-barrier heights for long-range electron transfer: insights from dyads with oligo-*p*-phenylene, oligo-*p*-xylene and oligo-*p*-dimethoxybenzene bridges. *Coord. Chem. Rev.* **254,** 2584–2592 (2010).
41. Laine, P. P., Bedioui, F., Loiseau, F., Chiorboli, C. & Campagna, S. Conformationally gated photoinduced processes within photosensitizer–acceptor dyads based on osmium(II) complexes with triarylpyridinio-functionalized terpyridyl ligands: insights from experimental study. *J. Am. Chem. Soc.* **128,** 7510–7521 (2006).
42. Meylemans, H. A., Lei, C. F. & Damrauer, N. H. Ligand structure, conformational dynamics, and excited-state electron delocalization for control of photoinduced electron transfer rates in synthetic donor–bridge–acceptor systems. *Inorg. Chem.* **47,** 4060–4076 (2008).
43. Sun, D. L., Rosokha, S. V., Lindeman, S. V. & Kochi, J. K. Intervalence (charge-resonance) transitions in organic mixed-valence systems. Through-space versus through-bond electron transfer between bridged aromatic (redox) centers. *J. Am. Chem. Soc.* **125,** 15950–15963 (2003).
44. Shen, J.-J. & Zhong, Y.-W. Long-range ruthenium–amine electronic communication through the para-oligophenylene wire. *Sci. Rep.* **5,** 13835 (2015).
45. Argazzi, R., Bignozzi, C. A., Heimer, T. A., Castellano, F. N. & Meyer, G. J. Enhanced spectral sensitivity from ruthenium(II) polypyridyl based photovoltaic devices. *Inorg. Chem.* **33,** 5741–5749 (1994).
46. Pavlishchuk, V. V. & Addison, A. W. Conversion constants for redox potentials measured versus different reference electrodes in acetonitrile solutions at 25 °C. *Inorg. Chim. Acta* **298,** 97–102 (2000).
47. Johansson, P. G. *et al.* Long-wavelength sensitization of TiO_2 by ruthenium diimine compounds with low-lying π^* orbitals. *Langmuir* **27,** 14522–14531 (2011).
48. Frisch, M. J. *et al. Gaussian 09* (Gaussian, Inc., 2009).
49. Robson, K. C. D. *et al.* Systematic modulation of a bichromic cyclometalated ruthenium(II) scaffold bearing a redox-active triphenylamine constituent. *Inorg. Chem.* **50,** 6019–6028 (2011).

Acknowledgements

The University of North Carolina (UNC) authors gratefully acknowledge support by a grant from the Division of Chemical Sciences, Office of Basic Energy Sciences, Office of Energy Research, US Department of Energy (DE-SC0013461). The University of British Columbia authors are grateful to the Canadian Natural Science and Engineering Research Council, Canadian Foundation for Innovation, Canadian Institute for Advanced Research and

Canada Research Chairs for support. The authors thank M. Gish and the Papanikolas group at UNC for the ultrafast measurements.

Author contributions

G.J.M., C.P.B. and K.H. proposed the ideas, A.D.B. and P.A.S. synthesized the compounds, K.H. and R.N.S. performed the electrochemical and photophysical experiments and K.H., R.N.S. and E.J.P. analysed the data. E.J.P. performed the Mulliken–Hush analysis, F.G.L.P. constructed Fig. 1 and G.J.M. wrote the manuscript with input from all the authors. G.J.M. and C.P.B. supervised the project.

Additional information

Supplementary information and chemical compound information are available in the online version of the paper. Reprints and permissions information is available online at www.nature.com/reprints. Correspondence and requests for materials should be addressed to G.J.M. and C.P.B.

Competing financial interests

The authors declare no competing financial interests.